Variable Frequency Phase-Shift Modulation Technique for Single Stage Dual-Active-Bridge AC-DC Converter

Dongxin Guo
School of Electrical Engineering and Automation
Harbin Institute of Technology
Harbin, China
guodongxin@stu.hit.edu.cn

Panbao Wang*
School of Electrical Engineering and Automation
Harbin Institute of Technology
Harbin, China
wangpanbao@hit.edu.cn

Chunguang Ren
Shanxi Key Lab. of Power System Operation and Control
Taiyuan University of Technology
Taiyuan, China
renchunguang@tyut.edu.cn

Josep M. Guerrero
Department of Energy Technology
Aalborg University
Aalborg, Denmark
joz@energy.aau.dk

***Abstract*-- This article proposes a variable frequency phase-shift modulation technique for single stage dual-active-bridge (DAB) AC-DC converter. This isolated single-stage single-phase converter consists of a DAB and a full bridge (FB) inverter. The proposed strategy applies a composite control strategy combining frequency modulation and extended phase shift (EPS) method to overcome the drawback of the non-linear power control of traditional phase-shift control scheme, which significantly reduces the complexity of the controller algorithm. Moreover, the synchronous inverter control applied to the back-end FB inverter is designed, which can realize the energy conversions in a single-stage, and a high frequency (HF) filter capacitor can replace the electrolytic capacitor at the output side DC-link. Thus, the safety of system operation improves and the power density of the system increases. Finally, simulation results confirm the validity and practical feasibility of the proposed control strategy.**

Index Terms*-- DAB AC-DC converter, DC-link HF filter capacitors, single-stage power control, extended phase shift control.

I. Introduction

With the rapid development of microgrids, isolated AC-DC converters are over a wide range of applications, including distributed generating systems, residential dc distribution systems, and electric vehicles [1]–[3]. With the extensive research and application of the above-mentioned applications, it is necessary to develop higher flexibility and higher efficiency bidirectional inverters.

In order to realize the function of galvanic isolation in many applications. A dual active bridge (DAB) should be cascaded at the front-end of the full-bridge (FB) inverter. Moreover, the high-frequency (HF) transformer can extend the voltage regulation range in different applications, and reduce the volume of the transformer by increasing the switching frequency [4]–[6]. Thus, the DAB AC-DC converter structure has been widely studied and adopted in power energy conversion application.

Dual-stage isolated inverters referred in [7] can realize bidirectional power transmission with a pretty good performance. However, connected with a power factor correcting as well as bulky failure prone electrolytic capacitors in the DC-side, the power density of the converter will be significantly reduced, causing the system to become heavy and bulkier. In order to realize high power density and high efficiency simultaneously, the single-stage approaches are preferred [8]–[11].

Whether the DAB is used for DC-DC, AC-DC or any other topology, the main goal is to promote the improvement of converter efficiency and power density. Improved modulation schemes include soft switching technology, eliminate reactive power, reducing current stress, and so on [12]–[14]. The basis of efficiency optimization control is the three degrees of freedom of DAB, including the inner phase shift angle of the primary FB, the inner phase shift angle of the secondary FB, and the outer phase shift angle between the primary and secondary FBs [15].

Single-phase-shift (SPS) has only one degree of freedom, and the method is simple [16]. However, SPS cannot optimize efficiency when the transferred power is determined. When the voltage amplitudes of two sides of the transformer do not match, the current stress and reactive power will be greatly increased, which leads to the increase in equipment costs and even damage to power devices [17]. In order to overcome the limitations of SPS control, the extended phase shift (EPS) control scheme is proposed [18]–[20], which can utilize the additional degrees of freedom to optimize the efficiency of the converter. The transferred power characterization of the EPS control scheme is analyzed in detail in [21]. Triple-phase-shift control (TPS) [22] has 3 control degrees of freedom, but TPS has 12 power modes and 8 switching states per switching cycle. Thus, the algorithm of the converter is realized based on EPS in this paper.

On the basis of the phase shift control, the efficiency optimization scheme is proposed in [23]. However, the traditional scheme using phase-shift control method will

lead to a nonlinear transferred power expression, which increases the complexity of the control and brings more troubles to the expansion of the converter [24]. An optimized modulation scheme that combines duty cycle, phase shift ratio, and switching frequency modulation is proposed in [25], which can achieve linearization between transferred power and control coordinates (i.e., phase shift ratio). However, this optimized scheme is based on the linear table interpolation, which cannot be implemented in the real-time digital microprocessors, and the control parameters must be obtained through table lookup. Then, difficulties arise to practical engineering applications. In addition, the extant DAB AC-DC optimal modulation scheme mainly focuses on the condition of forward power transfer mode, the reverse mode is not studied in these papers.

This paper is organized as follows. Sect. II introduces the variable frequency phase-shift modulation technique. Sect. III presents the simulation results of the proposed scheme based on the module built in the PLECS. Sect. IV draws some conclusions.

II. Variable Frequency Phase-Shift Modulation Technique

A. EPS control of the DAB AC-DC converter

The structure of the single-phase isolated bidirectional DAB AC-DC converter is shown in Fig.1. The front-stage DAB dc-dc converter includes an active full bridge FB_1 and an active full bridge FB_2. The inductor L is the total value of the transformer leakage inductor and the auxiliary inductor, and the turns ratio is 1:n. The C_2 is a small HF filter capacitor, cascaded with a FB inverter and output filter L_0.

The traditional two-stage control method applied in DAB AC-DC converters has higher requirements for stability of DC-side voltage, which leads to the widespread use of electrolytic capacitors. The electrolytic capacitor increases the failure rate of the converter while also increasing the volume of the converter. To overcome the drawback of the two-stage control method, a synchronous inverter control scheme is designed for the back-end FB inverter.

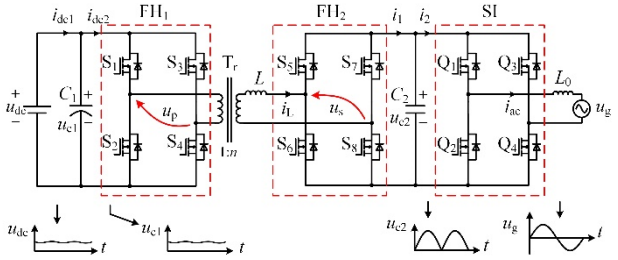

Fig. 1. Configuration of the single-phase single-stage bidirectional DAB AC-DC converter.

At steady state, the operating mode m_{FB} of the FB inverter changes two times each switching period of the u_g, according to

$$m_{SI}=\begin{cases}1 & \text{if } u_g>0 \ (Q_1,Q_4 \text{ are on})\\ -1 & \text{if } u_g<0 \ (Q_2,Q_3 \text{ are on})\end{cases} \quad (1)$$

The key waveforms of the converter with EPS control are shown in Fig. 2. T is the half switching period, and f_s (=1/(2T)) is the switching frequency of the front-stage DAB. D_1 is the phase shift ratio between S_1 and S_4, D_2 is the phase shift ratio between S_1 and S_5. The definition domain of D_1 and D_2 is: $0\le D_1\le 1$; $0\le D_2\le 1$. The duty cycle of all driving signals is 50%. We assume that t_0=0 at the beginning of the switching period. Define that $k=u_g/nu_{dc}$, and $k\le 1$ in this paper, another case $k>1$ can be analyzed similarly. The average current of inductance L in a switching period is zero in the steady state.

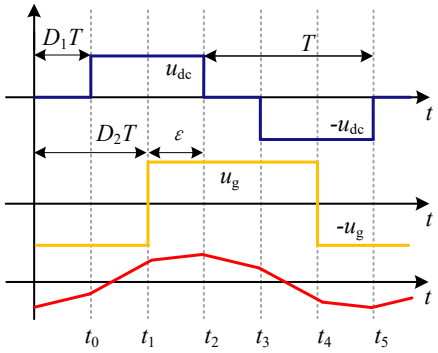

Fig. 2. Waveforms of the EPS modulation.

In the conventional control scheme, since the anti-parallel diode of switch Q_1 is reverse recovered and the parasitic capacitance of switch Q_2 starts to discharge when u_g becomes positive, a large voltage u_{c2} appears in inductor L_0. Therefore, a large current spike is generated at L_0 until the voltage of switch Q_4 drops to zero. As shown in Fig. 3, the switch Q_4 voltage is almost zero at the zero-crossing point of the inductor current i_g, which effectively suppresses large current spikes.

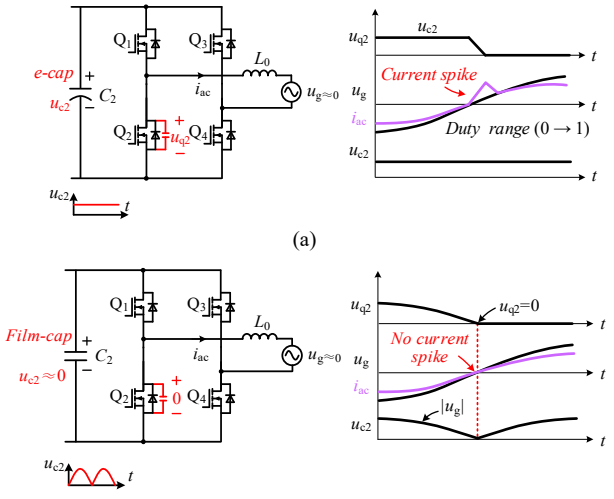

Fig. 3. Equivalent circuit and key waveforms showing the zero-crossing spike issue. (a) The conventional control method. (b) The proposed control method.

By analyzing the EPS modulation strategy, it can be derived that the inductance current at t_1, t_2 and t_3 is

$$i_{\mathrm{L}}(t_1)=\frac{nu_{\mathrm{dc}}T}{4L}[2D_1+k+4\varepsilon-1] \tag{2}$$

$$i_{\mathrm{L}}(t_2)=\frac{nu_{\mathrm{dc}}T}{2L}[1-2D_1+4D_1k+4\varepsilon k-k] \tag{3}$$

$$i_{\mathrm{L}}(t_3)=\frac{nu_{\mathrm{dc}}T}{2L}[1-2D_1+4\varepsilon k-k] \tag{4}$$

B. Variable Frequency Phase-Shift Modulation

Define the control coordinates ε=0.25(1-2D_1). Then the inner phase shift ratio can be expressed as D_1=0.5-2ε and the outer phase shift ratio can be expressed as D_2=0.5-ε, thus the control of the transferred power can be achieved by modulating ε.

In order to overcome the drawback of traditional phase shift control, the analytical scheme of the linear modulation scheme is necessary to be derived. The input current of FB inverter i_2 can be expressed as

$$i_2=\frac{1}{T}\int_{t_1}^{t_4} i_1(t)dt \tag{5}$$

According to (2)-(5), the input current of back-stage FB inverter can be derived as

$$i_2=\frac{nu_{dc}}{f_{\mathrm{s}}L}\varepsilon(1-2\varepsilon) \tag{6}$$

From (6), it is revealed that i_2 has a nonlinear relationship with the phase shift ratio ε, which increases the computational complexity. In order to simplify the algorithm, the switching frequency is defined as

$$f_{\mathrm{s}}=f_{\mathrm{n}}(1-2\varepsilon) \tag{7}$$

Note that f_{n} is the virtual switching frequency, which is a constant. The value of the actual frequency varies sinusoidally with time. Substituting (7) into (6), it can be obtained

$$i_2=\frac{nu_{\mathrm{dc}}}{f_{\mathrm{n}}L}\varepsilon \tag{8}$$

Assuming that I_{g} as the peak value of the AC-side current, thus u_{g}=U_{g}sin($\omega_{\mathrm{s}}t$), i_{ac}=I_{g}sin($\omega_{\mathrm{s}}t$), This paper defines that ε=M|sin($\omega_{\mathrm{s}}t$)|. Combining (8), the expression for optimal phase shift ratio can be expressed as

$$M=\frac{f_{\mathrm{n}}I_gL}{nu_{\mathrm{dc}}} \tag{9}$$

The instantaneous power of the converter can be derived as

$$\begin{aligned}p=u_{\mathrm{g}}i_{\mathrm{ac}}&=U_{\mathrm{g}}I_{\mathrm{ac}}\sin^2(\omega_{\mathrm{s}}t)=2P\sin^2(\omega_{\mathrm{s}}t)\\&=\frac{nu_{\mathrm{dc}}U_{\mathrm{g}}}{f_{\mathrm{n}}L}M\sin^2(\omega_{\mathrm{s}}t)\end{aligned} \tag{10}$$

Therefore, the average transferred power of the converter is derived as

$$P=\frac{nu_{\mathrm{dc}}U_{\mathrm{g}}}{2f_{\mathrm{n}}L}M \tag{11}$$

Since the voltage of AC-side and DC-side is invariable, the transmission power is positively correlated with the peak value of the phase shift ratio.

According to Table II, when the DC-side voltage is 400V, f_{n}=50kHz, L=185μH, and the voltage conversion ratio n=1, the relationship between the shift ratio ε and the switching frequency f_{s} for different amplitudes of the output current I_{g} are shown in Fig. 4. In Fig. 4, the left side of the vertical coordinate indicates the shift ratio ε and the right side indicates the switching frequency f_{s}. It can be seen that the amplitude of ε and f_{s} increases as the output current increases.

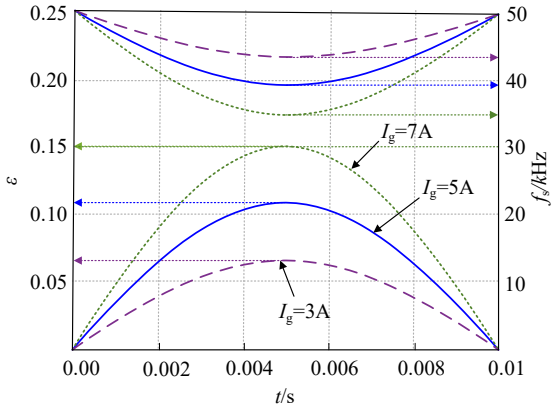

Fig. 4. Curve of phase shift ratio ε and switching frequency f_{s} with time.

The switching frequency range is an important basis for the selection of magnetic components, it can be deduced from (7) that the domain of definition of f_{s} is

$$f_{\mathrm{n}}/2\le f_{\mathrm{s}}\le f_{\mathrm{n}} \tag{12}$$

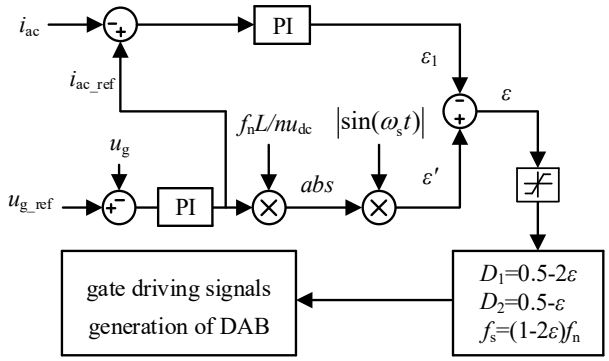

Fig. 5. The block diagram of variable frequency phase-shift modulation.

Fig. 5 plots the control block diagram of the isolated DAB AC-DC converter with variable frequency control. In order to maintain the stability of the voltage on the DC microgrid side, a voltage loop is set on the DC-side of the converter. The output signal of the voltage loop is the AC-side reference current $i_{\mathrm{ac\_ref}}$, which is substituted into (8) to obtain the main control coordinate ε'. The output parameter of current loop is the auxiliary control coordinate ε_1. The difference between the primary and auxiliary control coordinates is the phase shift ratio ε. The proposed algorithm controls the direction and magnitude of power transfer by modulating the current reference signal $i_{\mathrm{ac\_ref}}$. The regulation of the control coordinates does not vary with the power flow direction, thus the dynamic response of the proposed optimal modulation scheme is fast.

For the forward power transfer mode, the modulated signals of the front-end DAB are listed in Table I. The two switches of one leg have opposite modulated signals and the diagonal switches have the same modulated signal.

TABLE I
MODULATION SIGNAL FOR FORWARD MODE OF DAB

Modulation Parameters	Value
D_1	$0.5\text{-}2i_2f_nL/nu_{dc}$
D_2	$0.5\text{-}i_2f_nL/nu_{dc}$
f_s	$f_n(1\text{-}2i_2f_nL/nu_{dc})$

C. Analysis of the soft switching mode

When $i_L(t_1)>0$, S_5 and S_8 realize ZVS turn-on at t_1; when $i_L(t_2)>0$, S_2 realizes ZVS turn-on at t_2; when $i_L(t_3)>0$, S_3 realizes ZVS turn-on at t_3. According to the symmetry of inductor current at steady state, all switching devices of DAB AC-DC converter realize ZVS during full power range when the above three inequalities are satisfied at the same time. For the case that $k\leq 1$, considering the range of soft-switching operating and the peak value of the inductor current, define that $\varepsilon=0.25(1\text{-}2D_1)$. Combining with equation (9), the phase shift ratio ε can be derived as

$$\varepsilon = M\left|\sin(\omega_s t)\right| = \frac{f_n I_g L}{nu_{dc}}\left|\sin(\omega_s t)\right| \tag{13}$$

According to the above analysis, the coordinates of the phase shift ratio to achieve ZVS turn-on during the full operating range should satisfies (14).

$$\varepsilon \geq \frac{k}{4(1+k)} \tag{14}$$

Since $k=u_g/nu_{dc}=U_g|\sin(\omega_s t)|/nu_{dc}$, combining (13) and (14), the range of current values for the full range ZVS can be derived as

$$I_g \geq \frac{U_g}{4f_n L(1+U_g\left|\sin(\omega_s t)/nu_{dc}\right|)} \tag{15}$$

The range of instantaneous power for the full range ZVS condition can be obtained.

$$P \geq \frac{nu_{dc}\left|u_g\right|^2}{4f_n L(nu_{dc}+\left|u_g\right|)} \tag{16}$$

III. SIMULATION RESULT

To verify the feasibility of the proposed scheme, a DAB AC-DC converter module with the specifications in Table II was built in the PLECS. Simulation waveforms of the transferred power in different directions are given to demonstrate the theoretical analysis of the proposed modulation scheme.

Fig. 6 illustrates the simulation waveforms of the voltages on two sides of the inductor and the inductor current in millisecond for forward mode. Fig. 7 shows the waveforms of the output voltage u_g and output current i_{ac} for forward mode. As can be seen from Fig. 7, the proposed optimal control scheme effectively suppresses the zero-crossing current spike.

TABLE II
Main Parameters of the Module

Items	Descriptions	Specifications
u_{dc}	Input Voltage	400V
u_g	Output Voltage (RMS Value)	220V
p_{max}	Maximum power	2kW
n	Turn Ratio	1:1
L	Auxiliary Inductance	185μH
f_{ac}	Switching Frequency of SI	50Hz
f_n	Virtual Switching Frequency	50kHz
L_0	Filter Inductor	3mH
C_2	Film Capacitor	1μF

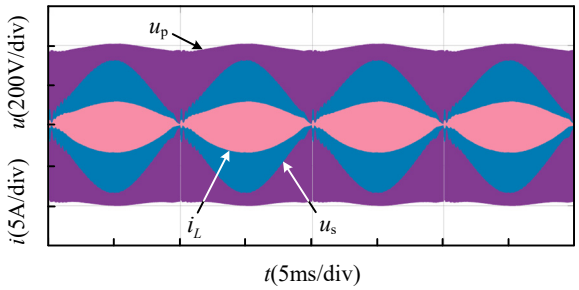

Fig. 6. The key waveform on the millisecond time scale.

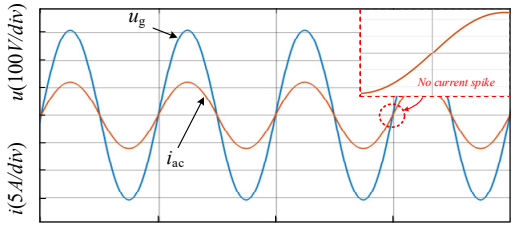

(a)

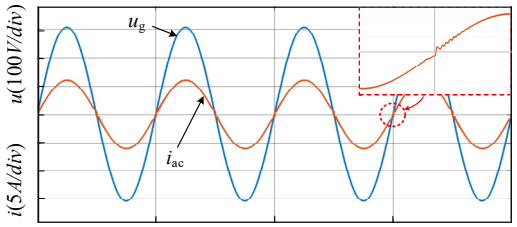

(b)

Fig. 7. Simulation waveforms of u_g and i_{ac} for forward mode. (a) Proposed scheme. (b) Conventional scheme.

Fig. 8 illustrates the operating waveforms of the converter controlled by the proposed scheme for forward mode and reverse mode. As can be seen from Fig.8, the optimized scheme linearizes the relationship between the control coordinate and the transferred power, which significantly reduces the complexity of the controller algorithm.

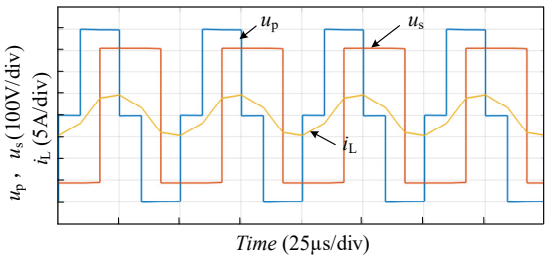

(a)

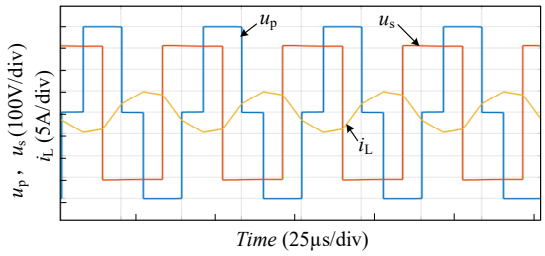

(b)

Fig. 8. Simulation waveforms of the proposed control method at the microsecond time scale. (a) Forward mod. (b) Reverse mode.

IV. Conclusions

This paper has detailed a variable frequency phase-shift modulation technique for single stage dual-active-bridge AC-DC converter. The optimized scheme linearizes the relationship between the control coordinate and the transferred power, which significantly reduces the complexity of the controller algorithm. In addition, the back-end FB adopts synchronous inverter control to achieve single-stage power control. Therefore, the electrolytic capacitor of the grid side is replaced by a film capacitor (i.e., C_2=1μF). As compared with the two-stage energy conversion method, the cost and size of the device are reduced and the reliability is improved. Furthermore, the current spike around ac voltage zero-crossing is eliminated due to the input voltage of the FB inverter is almost zero at zero-crossing point. Simulation verifications are carried out with bidirectional power transfer mode.

Acknowledgment

This work was supported by the Natural Science Foundation of Heilongjiang Province under Grant LH2022E067.

References

[1] Ahmed HMA, Eltantawy AB and Salama, MMA, “A Generalized Approach to the Load Flow Analysis of AC-DC Hybrid Distribution Systems,” *IEEE Transactions on Power Electronics*, vol. 33, no. 2, pp. 2117-2127, Mar. 2018.

[2] Ryu M H, Kim H S, Baek J W, Kim HG and Jung JH, “Effective Test Bed of 380-V DC Distribution System Using Isolated Power Converters,” *IEEE Transactions on Industrial Electronics*, vol. 62, no. 7, pp. 4525-4536, Jul. 2015.

[3] Das D, Weise N, Basu K, Baranwal R and Mohan N, “A Bidirectional Soft-Switched DAB-Based Single-Stage Three-Phase AC-DC Converter for V2G Application,” *IEEE Transactions on Industrial Electronics*, vol. 5, no. 1, pp. 189-199, Mar. 2019.

[4] G. K. Y. Ho, Y. Fang and B. M. H. Pong, "A Multiphysics Design and Optimization Method for Air-Core Planar Transformers in High-Frequency LLC Resonant Converters," *IEEE Transactions on Industrial Electronics*, vol. 67, no. 2, pp. 1605-1614, Feb. 2020.

[5] Z. Guo, A. Q. Huang, R. E. Hebner, G. C. Montanari and X. Feng, "Characterization of Partial Discharges in High-Frequency Transformer Under PWM Pulses," *IEEE Transactions on Power Electronics*, vol. 37, no. 9, pp. 11199-11208, Sept. 2022.

[6] M. A. Sayed, K. Suzuki, T. Takeshita and W. Kitagawa, "PWM Switching Technique for Three-Phase Bidirectional Grid-Tie DC–AC–AC Converter With High-Frequency Isolation," *IEEE Transactions on Power Electronics*, vol. 33, no. 1, pp. 845-858, Jan. 2018.

[7] Qin HS and Kimball JW, “Closed-Loop Control of DC-DC Dual-Active-Bridge Converters Driving Single-Phase Inverters,” *IEEE Transactions on Power Electronics*, vol. 29, no. 2, pp. 1006-1017, Feb. 2014.

[8] P. Ma, D. Sha and K. Song, "A Single-Stage Semi Dual-Active-Bridge AC–DC Converter With Seamless Mode Transition and Wide Soft-Switching Range," *IEEE Transactions on Industrial Electronics*, vol. 70, no. 2, pp. 1387-1397, Feb. 2023.

[9] Y. Zhang, G. Yang, J. Li, Z. Kong and X. Zhu, "A Modulation Scheme With Full Range ZVS and Natural Power Factor Correction for Bridgeless Single-Stage Isolated AC–DC Converter," *IEEE Transactions on Power Electronics*, vol. 38, no. 1, pp. 195-205, Jan. 2023.

[10] T. Chen, R. Yu and A. Q. Huang, "Variable-Switching-Frequency Single-Stage Bidirectional GaN AC–DC Converter for the Grid-Tied Battery Energy Storage System," *IEEE Transactions on Industrial Electronics*, vol. 69, no. 11, pp. 10776-10786, Nov. 2022.

[11] W. Uddin, T. A. Wagaye and M. Kim, "Quasi-Single-Stage Current-Fed Resonant AC–DC Converter Having Improved Heat Distribution," *IEEE Transactions on Power Electronics*, vol. 37, no. 11.

[12] G. Xu, L. Li, X. Chen, W. Xiong, X. Liang and M. Su, "Decoupled EPS Control Utilizing Magnetizing Current to Achieve Full Load Range ZVS for Dual Active Bridge Converters," *IEEE Transactions on Industrial Electronics*, vol. 69, no. 5, pp. 4801-4813, May 2022.

[13] H. Bai and C. Mi, "Eliminate Reactive Power and Increase System Efficiency of Isolated Bidirectional Dual-Active-Bridge DC–DC Converters Using Novel Dual-Phase-Shift Control," *IEEE Transactions on Power Electronics*, vol. 23, no. 6, pp. 2905-2914, Nov. 2008.

[14] Z. Guo and X. Han, "Control Strategy of AC-DC Converter Based on Dual Active Bridge With Minimum Current Stress and Soft Switching," *IEEE Transactions on Power Electronics*, vol. 37, no. 9, pp. 10178-10189, Sept. 2022.

[15] Y. Zhuang et al., "A Peak Current Reducing Method for Input-Independent and Output-Series Modular Converters With LC-Branch-Based Power Balancing Unit," *IEEE Transactions on Industrial Electronics*, vol. 70, no. 1, pp. 418-429, Jan. 2023.

[16] F. Krismer and J. W. Kolar, “Accurate Small-Signal Model for the Digital Control of an Automotive Bidirectional Dual Active Bridge,” *IEEE Transactions on Industrial Electronics*, vol. 24, no. 12, pp. 2756–2768, Dec. 2009.

[17] Zhang JK, Sha DS and Ma PS, “A Dual Active Bridge DC-DC-Based Single Stage AC-DC Converter With Seamless Mode Transition and High Power Factor,” *IEEE Transactions on Industrial Electronics*, vol. 69, no. 2, pp. 1411-1421, Feb. 2022.
[18] G G Oggier, G O Garcia, and A R Oliva, “Modulation strategy to operate the dual active bridge DC-DC converter under soft switching in the whole operating range,” *IEEE Transactions on Power Electronics*, vol. 26, no. 4, pp. 1228–1236, Apr. 2011.
[19] H. Shi et al., "Minimum-Backflow-Power Scheme of DAB-Based Solid-State Transformer With Extended-Phase-Shift Control," *IEEE Transactions on Industry Applications*, vol. 54, no. 4, pp. 3483-3496, July-Aug. 2018.
[20] G. Xu, L. Li, X. Chen, Y. Liu, Y. Sun and M. Su, "Optimized EPS Control to Achieve Full Load Range ZVS With Seamless Transition for Dual Active Bridge Converters," *IEEE Transactions on Industrial Electronics*, vol. 68, no. 9, pp. 8379-8390, Sept. 2021.
[21] Hou N, et al, “Minimum-Current-Stress Scheme of Dual Active Bridge DC-DC Converter With Unified Phase-Shift Control,” *IEEE Transactions on Power Electronics*, vol. 31, no. 12, pp. 8552-8561, Dec. 2016.
[22] L. Chen et al., "Moving Discretized Control Set Model-Predictive Control for Dual-Active Bridge With the Triple-Phase Shift," *IEEE Transactions on Power Electronics*, vol. 35, no. 8, pp. 8624-8637, Aug. 2020.
[23] Y. Tang et al., "Reinforcement Learning Based Efficiency Optimization Scheme for the DAB DC–DC Converter With Triple-Phase-Shift Modulation," *IEEE Transactions on Industrial Electronics*, vol. 68, no. 8, pp. 7350-7361, Aug. 2021.
[24] Cho YW, Cha WJ, Kwon JM and Kwon BH, “High-Efficiency Bidirectional DAB Inverter Using a Novel Hybrid Modulation for Stand-Alone Power Generating System With Low Input Voltage,” *IEEE Transactions on Power Electronics*, vol. 31, no. 6, pp. 4138–4147, Jun. 2016.
[25] Everts J, Krismer F, Van den Keybus J, Driesen J and Kolar JW, “Optimal ZVS Modulation of Single-Phase Single-Stage Bidirectional DAB AC-DC Converters,” *IEEE Transactions on Power Electronics*, vol. 29, no. 8, pp. 3954–3970, Aug. 2014.